Direct Observation of Geometrical Phase Transitions in Mesoscopic Superconductors by Scanning Tunneling Microscopy

G. Karapetrov,[1] J. Fedor,[1,2] M. Iavarone,[1] D. Rosenmann,[1] and W. K. Kwok[1]

[1]*Materials Science Division, Argonne National Laboratory, Argonne, Illinois 60439, USA*

[2]*Institute of Electrical Engineering, Slovak Academy of Sciences, Dúbravská cesta 9, 84104 Bratislava, Slovakia*

(Received 6 May 2005; published 10 October 2005)

Using scanning tunneling microscopy, we mapped the distribution of the local density of states in a single crystal superconductor heterostructure with an array of submicron normal metal islands. We observe the coexistence of strongly interacting multiquanta vortex lattice with interstitial Abrikosov vortices. The newly formed composite magnetic flux structure undergoes a series of phase transitions between different topological configuration states. The vortex configuration states are strongly dependent on the number of flux quanta and the nanoscale confinement architecture of the mesoscopic superconductor. Here, we present images of vortex phase transitions due to confinement effects when the number of magnetic flux quanta in the system changes. The vortex dynamics in these systems could serve as a model for behavior of confined many-body systems when the number of particles changes.

DOI: 10.1103/PhysRevLett.95.167002 PACS numbers: 74.50.+r, 74.25.Jb, 74.25.Qt

When homogeneous type-II superconductors are subjected to an external magnetic field, the Abrikosov vortices, each with a radius ξ and carrying a single flux quantum Φ_0, form a triangular lattice. The lattice structure has been observed by magnetic decoration, scanning tunneling microscopy, neutron scattering, and scanning Hall probe microscopy [1–3]. In homogenous superconductors, the formation of multiquanta vortices is unfavorable [4]. On the other hand, when the superconductor has antidots (holes) with a size r larger than 2ξ, multiquanta vortices could form inside the antidots with maximum flux quanta reaching up to the saturation value $n_s = r/2\xi$ [5]. The first indications of such behavior were reported by Hebard *et al.* [6] from the measurement of the bulk transport current in samples with periodic defects. Scanning tunneling spectroscopy (STS) could directly image vortex structures in superconductors with very high spatial resolution since it discriminates individual vortex structures by measuring variations of the local density of states on the surface. This advantage of STS could be exploited to directly image the topological states of the vortex lattice in mesoscopic structures at high magnetic fields where size effects play a critical role and vortex-vortex interaction is strong. So far, the rigorous requirement of surface quality for STS has been an insurmountable obstacle in achieving images of vortices in superconductors with engineered mesoscopic periodic pinning sites. Here we report on direct visualization of vortex phase transitions in a mesoscopic superconductor-normal metal heterostructure.

$NbSe_2$ single crystals were grown in evacuated quartz ampoules by an iodine vapor transport method [7]. Flat samples with sizes of up to $10 \times 10 \times 0.1$ mm^3 were characterized by x-ray, transport, and magnetization measurements. SQUID magnetization measurements show typical superconducting transitions of 7.2 K with transition width of 10 mK. As-grown single crystals were cleaved to expose a clean flat surface. Using a focused beam of gallium ions, we etched a set of 1 μm deep parallel grooves spaced equidistantly 0.5 μm apart. A second set of identical grooves, orthogonal to the original one, was inscribed in the same area. Two micrometers of gold was electroplated on the patterned surface. The undisturbed backside of the patterned single crystal of $NbSe_2$ was subsequently cleaved several times until the underlying electroplated gold pattern was uncovered [Figs. 1(a) and 1(b)]. The latter procedure was performed in an inert atmosphere of helium gas to avoid contamination of the freshly exposed $NbSe_2$ surface. This method produces a clean, atomically flat $NbSe_2$ single crystal surface which is imbedded with laterally patterned submicron gold islands. The sample was then immediately transferred into a low-temperature scanning tunneling microscope and cooled down to 4.2 K. This novel approach in fabricating patterned crystal heterostructures with atomically flat single crystal surfaces free of contaminants is a key requirement to obtain vortex images with scanning tunneling spectroscopy.

An STM topographic image taken on a 2×1.4 μm^2 area shows that the crystal surface consists of atomically flat regions filled with a periodic array of elliptical gold islands [Fig. 1(c)]. Using STS we can measure the local conductance and thus determine the local density of states at every point on the surface. A typical set of STS spectra along a line leading to the center of the Au island is shown in Fig. 1(d). The tunneling conductance spectra taken between the holes show the typical superconducting gap of $NbSe_2$ at 4.2 K with a superconducting energy gap value of 1.0 meV. On the other hand, the spectrum taken in the middle of the ellipse shows gapless conductance of a normal metal—a signature of the presence of gold.

To search for Abrikosov vortices in the superconductor, we performed conductance map of the same area as in

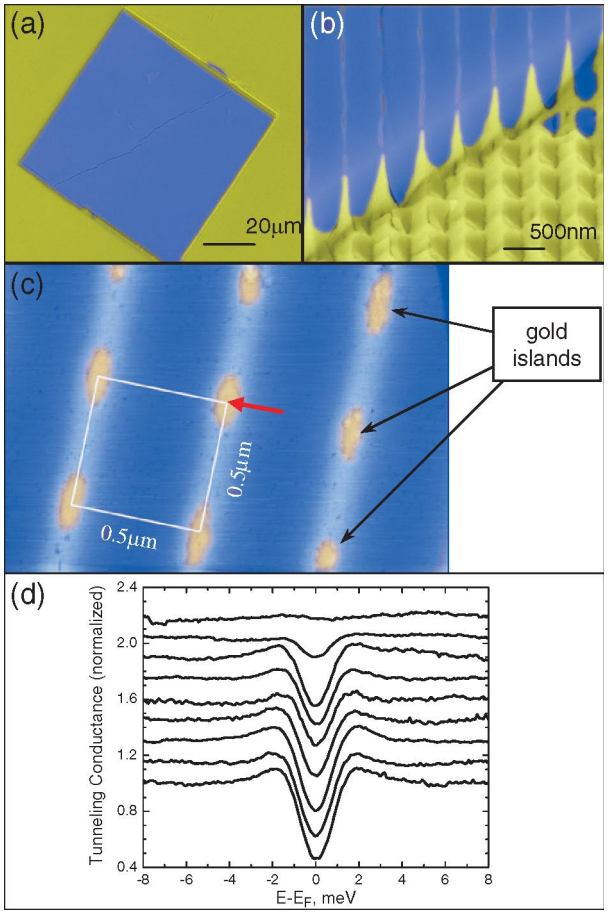

FIG. 1 (color). (a),(b) Scanning electron micrographs (colorized) of the patterned $NbSe_2$ single crystal, and (c),(d) scanning tunneling topography and spectroscopy. (a) Top view of the periodic structure containing a square array of 130×130 islands. The yellow area contains the electroplated gold, and the blue area represents the patterned $NbSe_2$ single crystal. (b) 45° view of the sample's cross section after performing a cross-sectional cut using FIB. (c) Scanning tunneling microscopy of the patterned $NbSe_2$ single crystal (2×1.4 μm^2) at 4.2 K. The red arrow indicates the locations where the tunneling spectroscopy curves shown in (d) were acquired. The scanning tunneling spectroscopy was performed using a 0.2 GΩ junction at 20 mV bias voltage in zero applied magnetic field at 4.2 K. For clarity purposes, the curves are offset vertically by 0.15 a.u. as the tip approached the elliptical island.

Fig. 1. Imaging vortices by STS is based on the fact that there are gap states inside a vortex core, and therefore the quasiparticle tunneling conductance spectrum exhibits an increase around the Fermi energy. The main difference in conductance curves inside and outside the vortex core is at the Fermi level ($V_{bias} = 0$ V) and near the superconducting gap peak ($V_{bias} = \pm 2.0$ meV). We performed a conductance map at $V_{bias} = +2.0$ meV, which resulted in superconducting areas having higher conductance (red areas) than the gapless regions (blue areas). A typical local density of states (LDOS) map in zero applied magnetic field is shown in Fig. 2(a). The image shows that the periodic array of elliptical islands has a lower conductance consistent with the spatially dependent tunneling spectra shown in Fig. 1(d). The gapless tunneling spectra inside the island indicate that they consist of a normal metal. The square periodicity of the array of submicron Au islands forms an ideal periodic trapping potential for the Abrikosov vortex lattice [8,9]. The first matching field, a condition when each island contains one magnetic flux quantum, is 8.28 mT.

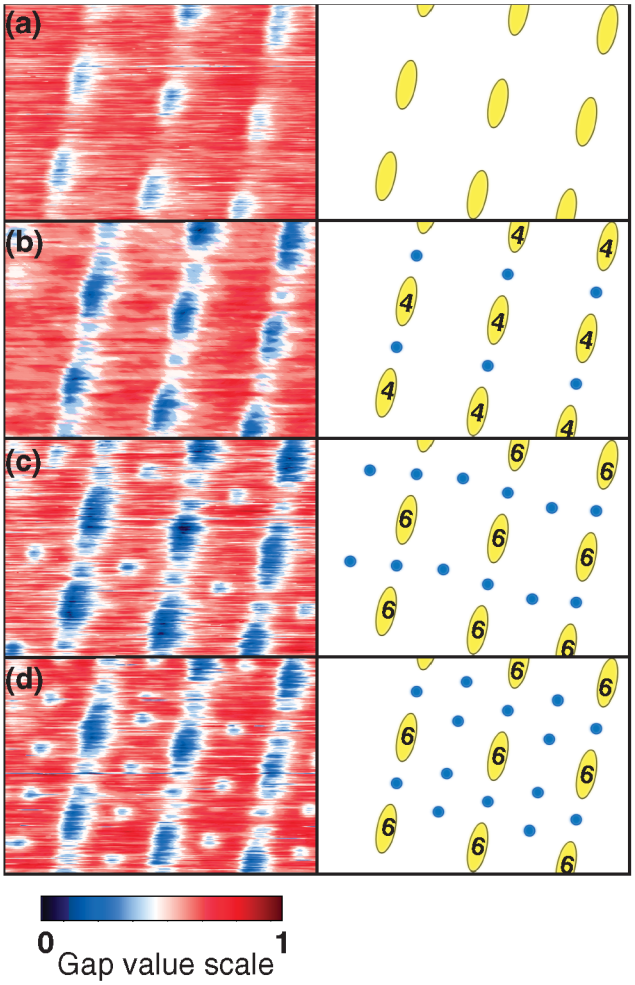

FIG. 2 (color). Current image tunneling spectroscopy images and schematics of the vortex configurations in a square array of normal metal elliptical holes at matching magnetic fields of (a) $H = 0$, (b) $H = 5H_0$, (c) $H = 8H_0$, and (d) $H = 9H_0$, where H_0 is the matching field of 8.28 mT. Scanning tunneling spectroscopy images were taken at the $NbSe_2$ superconducting peak energy $E_g = +2.0$ meV on an area 1.4×2.0 μm^2 at 4.2 K. Color scale represents regions with enhanced superconductivity (red) and suppressed superconducting order parameter (blue). Yellow ellipses in the schematic images represent the nonsuperconducting elliptical holes containing multiquanta vortices. Blue dots represent single-quanta Abrikosov vortices. The two sublattices form regular configurations at matching fields.

Next, we apply a magnetic field which slightly exceeds the first matching field and obtain a conductance map that images the vortex distribution in this periodically modulated confined system. The LDOS inside the gapless Au antidot is not expected to change in the presence of a single or multiquanta vortex residing on the antidot. Indeed, even at applied magnetic fields exceeding 3 times the matching field, we do not observe any vortices in the area between the normal metal islands, and the size and contrast of the normal areas remain the same. This indicates that the magnetic field penetrates the superconductor through the normal state Au antidots, at first forming single-quanta vortices and subsequently, at higher fields, multiquanta vortex states. Considering the temperature dependent in-plane coherence length in this superconductor at 4.2 K to be 12.4 nm, we estimate the magnetic flux saturation number n_s for an individual ellipse to be 6. Indeed, we observe the appearance of single-quanta (Abrikosov) vortices in the interstitial regions between the Au islands [Fig. 2(b)] only when the magnetic field is further increased up to 42 mT (i.e., slightly above the fifth matching field). At this field, we observe the coexistence of a regular square lattice of multiquanta vortices and a square lattice of single-quanta Abrikosov vortices with the same periodicity, but shifted by a half period with respect to the multiquanta lattice. The interpenetrating lattices are stabilized by the volume distribution of the LDOS, the repulsive vortex-vortex interaction, and Meissner currents acting on the magnetic flux system. Each gold ellipse containing 4-Φ_0 flux strongly repels the single-quanta interstitial Abrikosov vortices. The Abrikosov vortices, on the other hand, are squeezed towards the center of the sample by the Meissner currents distributed around the perimeter of the crystal. The Abrikosov vortices can move in between the array of ellipses and find their equilibrium positions to minimize their total energy. The energy per unit length of the Abrikosov vortex is comprised of two terms: the vortex self-energy comprising the magnetic and nonsuperconducting core contributions and the repulsive interaction energy with other vortices [10]:

$$F = \left(\frac{\Phi_0}{4\pi\lambda}\right)^2\left(\ln\kappa + \frac{1}{2}\right) + \sum_n \frac{n}{2}\left(\frac{\Phi_0}{2\pi\lambda}\right)^2 K_0\left(\frac{x - x_n}{\lambda}\right), \quad (1)$$

where λ is the superconducting penetration depth, $\kappa = \frac{\lambda}{\xi}$, n is the number of flux quanta of the nearby interacting vortex, and K_0 is the zero-order MacDonald function. The first energy contribution is influenced by the single crystal's periodic thickness modulation in the interstitial regions favoring vortex accommodation in areas where the sample is thinner or has suppressed superconducting properties. The second part is determined by the Abrikosov vortex repulsive interaction with the periodic array of elliptical islands saturated with magnetic flux and the interaction with other Abrikosov vortices.

At the fifth matching field, the single Abrikosov vortex per unit cell is accommodated at the position alongside the elliptical holes with 4-Φ_0 flux [Fig. 2(b)]. The choice to reside at this position signifies the prevailing energy gain due to a shortening of the vortex length in the very thin $NbSe_2$ layer between the holes over the increased energy due to enhanced magnetic interaction with the multiquanta vortices at this particular accommodation site.

The second Abrikosov vortex in the unit cell appears when the magnetic field reaches the eighth matching field. The sixth and seventh matching fields add flux quanta into the multiquanta vortex on the Au islands causing a transition from 4-Φ_0 to 5-Φ_0 and from 5-Φ_0 to 6-Φ_0, respectively. This brings the antidot into saturation, so that any further increase of applied magnetic field produces interstitial single-quanta Abrikosov vortices. The new vortices get squeezed in between the existing square lattice of Abrikosov vortices [Fig. 2(c)]. The repulsive force from the multiquanta lattice and the existing interstitial Abrikosov vortices drives the second interstitial vortex into the $(1/2, 1/2)$ coordinate position with respect to the multiquanta lattice. It is remarkable that even at the eighth matching field, the ordering is close to perfect at temperatures $T/T_c \sim 0.6$—clear evidence of the dominant role of vortex-vortex interactions over the intrinsic pinning in this high-quality $NbSe_2$ single crystal.

Further increase of the applied magnetic field leads to an increase in the number of Abrikosov vortices. The elliptical pinning centers start to define superconducting ''channels'' where the Abrikosov vortices can freely move and adopt the configuration that minimizes the total energy of the combined system of multiquanta and Abrikosov vortices. Although similar ''channel'' configurations have been considered earlier to study vortex motion and pinning [11–14] in mesoscopic superconductors, no direct experimental evidence of geometrical transitions have been found. When higher magnetic fields are applied, the number of Abrikosov vortices in our channel increases and forms a single chain parallel to the major axis of the elliptical pinning centers [Fig. 3(a)]. At this point the interaction between the Abrikosov vortices in each channel becomes strong and determines their distribution within the channel. The chains consist of periodically spaced vortices positioned in the middle of the superconducting channels. As the external magnetic field increases, so does the vortex density. This process takes place continuously up to a critical point where a new geometrical configuration becomes more energetically favorable. At this critical vortex density, a geometrical phase transition occurs when a linear chain splits into a double chain [Fig. 3(b)]. This transition originates from the mesoscopic one-dimensional confinement of the vortex motion. The mesoscopic property of the system is linked to the width of the confining channel where the vortices are restricted to move only along the channel. The confinement is on the order of the

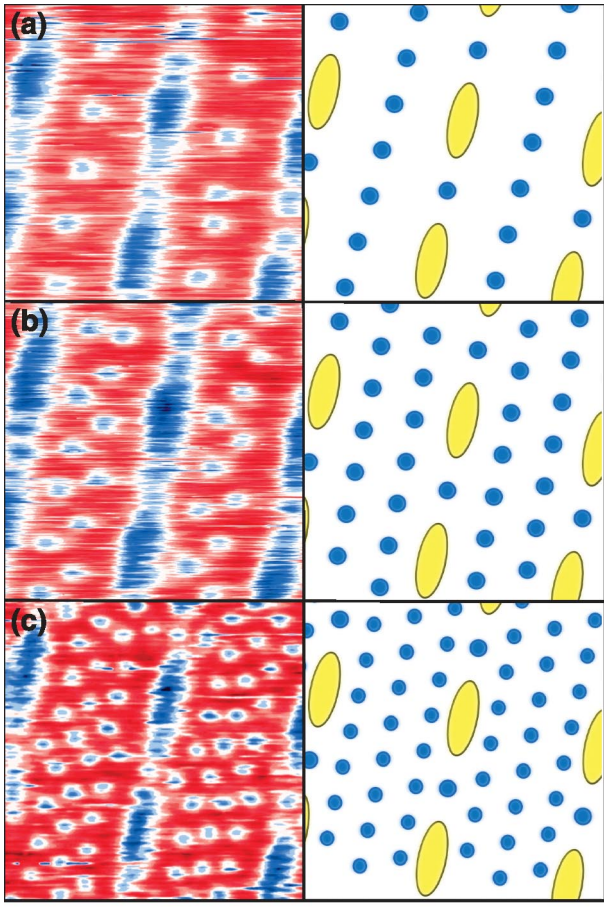

FIG. 3 (color). Images of vortex geometrical transitions in the periodic array of pinning centers using current image tunneling spectroscopy (left panels) and corresponding schematic distributions (right panels) on an area of 1.25×1.25 μm^2 at 4.2 K. The applied magnetic field varies from (a) 82.5 mT, (b) 120 mT to (c) 212.5 mT.

magnetic size of the vortex—the penetration length. This confinement of the Abrikosov vortex system in one dimension leads to quantized geometrical configurations with distinct symmetries that transition at specific magnetic fields. As the magnetic field is further increased, the intrachain vortex separation decreases while the interchain distance remains constant. At higher fields, when the intervortex separation within a chain reaches a critical value equal to one-quarter of the channel width, the double-chain system transitions into a triple chain [Fig. 3(c)], splitting the superconducting channel into four equal parts. Similar transitions were first predicted by Guimpel *et al.* [15] and Brongersma *et al.* [16], and this is the first experimental evidence confirming the chain configurations. We observe that the nucleation of the vortex chains occurs through the development of kinks in the linear chain. Like any thermodynamic phase transition, this one nucleates the new phase at the defect sites located at the boundaries of the superconducting channel and propagates into the channel through the vortex chains.

These studies elucidate the microscopic mechanism of topological vortex phase transitions in mesoscopic superconductors. Direct imaging of the coexistent lattices of multiquanta vortices and single quantum Abrikosov vortices highlights the complex nature of the interaction between the two magnetic sublattices that leads to enhanced current carrying characteristics of superconductors with nanoscale defect patterns.

We would like to acknowledge M. Marshall and the Center for Microanalysis of Materials at University of Illinois, Urbana-Champaign, for support with the focus ion beam instrumentation. We would also like to thank R. Divan of the CNM, ANL, and M. Moldovan (Northwestern, Evanston, IL) for their help with sample preparation and A. E. Koshelev and V. Vlasko-Vlasov for useful discussions. Part of this work was carried out in the Center for Microanalysis of Materials, University of Illinois at Urbana-Champaign, which is partially supported by the U.S. Department of Energy under Grant No. DEFG02-91-ER45439. This work has been supported by the U.S. DOE, BES-Material Sciences under Contract No. W-31-109-ENG-38.

[1] A. Oral, S. J. Bending, and M. Henini, Appl. Phys. Lett. **69**, 1324 (1996).
[2] G. J. Dolan, F. Holtzberg, C. Field, and T. R. Dinger, Phys. Rev. Lett. **62**, 2184 (1989).
[3] H. F. Hess, R. B. Robinson, and J. V. Waszczak, Phys. Rev. Lett. **64**, 2711 (1990).
[4] A. A. Abrikosov, Sov. Phys. JETP **5**, 1174 (1957).
[5] G. S. Mkrtchyan and V. V. Shmidt, Sov. Phys. JETP **34**, 195 (1972).
[6] A. F. Hebard, A. T. Fiory, and S. Somekh, IEEE Trans. Magn. **13**, 589 (1977).
[7] C. S. Oglesby *et al.*, J. Cryst. Growth **137**, 289 (1994).
[8] M. Baert *et al.*, Europhys. Lett. **29**, 157 (1995).
[9] V. V. Moshchalkov *et al.*, Phys. Rev. B **54**, 7385 (1996).
[10] M. Tinkham, *Introduction to Superconductivity* (Krieger Publishing, Malabar, FL, 1975).
[11] M. O. Andre *et al.*, Physica (Amsterdam) **338C**, 179 (2000); N. Kokubo *et al.*, Phys. Rev. Lett. **88**, 247004 (2002).
[12] I. V. Grigorieva *et al.*, Phys. Rev. Lett. **92**, 237001 (2004).
[13] G. Stan, S. B. Field, and J. M. Martinis, Phys. Rev. Lett. **92**, 097003 (2004).
[14] C. Reichhardt, G. T. Zimanyi, and N. Gronbech-Jensen, Phys. Rev. B **64**, 014501 (2001).
[15] J. Guimpel *et al.*, Phys. Rev. B **38**, 2342 (1988).
[16] S. H. Brongersma *et al.*, Phys. Rev. Lett. **71**, 2319 (1993).